Carrier Transport in a Deep Ultraviolet Mixed Quantum Well Light Emitting Diode

Friedhard Römer, Gregor Hofmann, Jakob Höpfner, Marcel Schilling, Anton Muhin, Tim Wernicke, Michael Kneissl, *Fellow, IEEE*, and Bernd Witzigmann, *Senior Member, IEEE*

***Abstract*—Aluminium Gallium Nitride (AlGaN) based light emitting diodes (LED) are the enabling technology for compact emitters of deep ultraviolet (DUV) radiation and are in high demand for environmental and medical applications. The efficiency of recent DUV LEDs is in the range of a few percent providing some potential for improvement. Apart from the light extraction efficiency the hole injection into the active region presents a major obstacle towards more efficient DUV LEDs. In this work, we investigate the emission spectra of a mixed multi quantum well (MQW) DUV LED to attain details on the active region carrier transport that allow an improvement of the hole injection. Changing the position of the long wavelength marker quantum well yields characteristic emission spectra which have been modelled with a multi scale carrier transport and luminescence simulator. The numerical modelling enables the extraction of opaque carrier transport characteristics in AlGaN such as the hole mobility in the highly doped barriers of the MQW.**

***Index Terms*—Light emitting diode, deep ultraviolet, carrier transport, III-Nitride, numerical modelling.**

I. Introduction

COMPACT deep ultraviolet (DUV) emitters with simple power requirements that enable battery operation are in high demand for applications such as water purification, medical treatment, and material processing amongst others [1]. These requirements cannot be fulfilled by conventional incandescent or gas discharge sources of DUV radiation. Recent advances in the III-Nitride technology have facilitated the implementation of DUV light emitting diodes (LED) made of Aluminium Gallium Nitride (AlGaN) which lend themselves for this purpose. Despite the progress made so far the wall plug efficiency (WPE) is quite low at about 10% for LEDs emitting at 270 nm wavelength dropping to less than 1% at 235 nm [2]. Thus, there is still some potential for improvement.

Manuscript received 1 December 2023; revised 4 January 2024; accepted 5 January 2024. Date of publication 10 January 2024; date of current version 24 January 2024. This work was supported by the Leibniz Association joint project UVSimTech under the contract K415/2021. *(Corresponding author: Friedhard Römer.)*

Friedhard Römer, Gregor Hofmann, and Bernd Witzigmann are with Lehrstuhl für Optoelektronik, Department EEI, Friedrich-Alexander-Universität Erlangen-Nürnberg, D-91052 Erlangen, Germany (e-mail: friedhard.roemer@fau.de).

Jakob Höpfner, Marcel Schilling, Anton Muhin, Tim Wernicke, and Michael Kneissl are with the Institut für Festkörperphysik, Technische Universität Berlin, D-10623 Berlin, Germany.

Digital Object Identifier 10.1109/JPHOT.2024.3351965

The efficiency of recent DUV LEDs suffers particularly from low light extraction efficiency (LEE) and carrier injection efficiency (CIE) into the active region. Light extraction in DUV LEDs is subject to increased contribution of TM-polarized emission below 265 nm wavelength [3] and high absorption of materials, particularly the p-side material. The CIE suffers from the low hole injection efficiency into the active region. Isolated Magnesium (Mg) sites acting as acceptor dopants have an ionization energy $E_A > 0.7$ eV in AlN [4]. The ionization energy reduces with the proximity effect [5] but the free hole density in Mg doped AlGaN with high Al content remains as low as $p \approx 10^{16}\,\mathrm{cm}^{-3}$. The hole mobility in AlN is $\mu_{\mathrm{h,AlN}} \approx 1\,\mathrm{cm}^2/(Vs)$ and decreases strongly with increasing dopant density [6]. Apart from increasing the p-side resistance the hole mobility affects the hole injection into the active region as discussed in Section IV.

Recent III-Nitride semiconductor technology permits Silicon donor doping in $\mathrm{Al}_x\,\mathrm{Ga}_{1-x}\mathrm{N}$ with up to $x \approx 84\%$ Al content [2], [7]. Above this value the free electron density strongly decreases setting a limit for the Al content and thus the band gap in the n-side and the active region. Quantum wells (QW) approaching $x_{\mathrm{QW}} \lesssim 84\%$ are rather shallow promoting electron overshoot. The p-side electron barrier is limited to pure AlN and becomes less effective with higher Al content in the barriers.

DUV AlGaN LEDs are prone to inhomogeneous broadening (IHB) caused by alloy fluctuations [8]. The IHB has been connected with an S-shaped curve of the photon energy versus temperature in photoluminescence experiments and a residual emission bandwidth at cryogenic temperatures [9], [10]. The modification of the phase space filling caused by the IHB affects the carrier transport [11]. This effect cannot be neglected in DUV AlGaN LEDs where the IHB is often much larger than $k_B T$.

Despite these findings the carrier injection and active region carrier transport in an AlGaN DUV multi quantum well (MQW) LED is not yet well understood impeding the model based design optimization of the active region and hole injection structure. To attain access to the active region carrier transport we investigate a mixed triple QW DUV LED with two QW emitting at 233 nm and one QW emitting at 250 nm. Moving the position of the 250 nm QW then facilitates the analysis of the carrier transport by the spectral signature. This has been demonstrated for visible III-Nitride LED [12], [13]. In the analysis we combine characterization results and numerical modelling to analyze the hole injection and carrier transport within the active region. The mixed MQW LED implementation and the multi scale transport

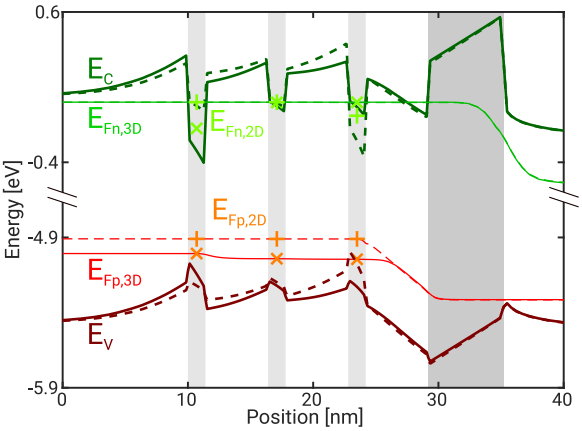

Fig. 1. Band structure of the N-MQW (solid) and P-MQW (dashed) at $T = 300$ K and $j = 13$ Acm^{-2}. The thin lines illustrate the continuum Fermi levels. The markers show the bound Fermi levels in the N-MQW ($\times$) and P-MQW ($+$).

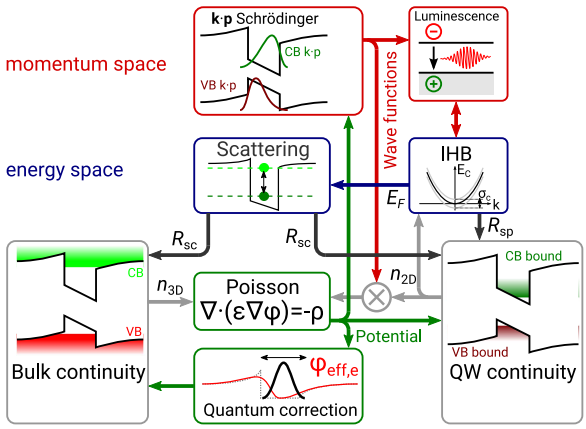

Fig. 2. Physical models and their interaction of the multi scale transport simulator.

simulation model are outlined in Section II. The model calibration and the carrier transport in the active region are discussed in the Sections III and IV and finally assessed in Section V.

II. Mixed MQW LED Simulation Model

The simulation model of the mixed MQW structure closely resembles its realization [14]. The active region is made of three 1.4 nm wide quantum wells (QW) separated by 5 nm wide $Al_{0.83}Ga_{0.17}N$ barriers. The n-side composition is $Al_{0.87}Ga_{0.13}N$. The p-side barrier is followed by an intrinsic 6 nm wide AlN electron blocking layer (EBL). The following Mg doped superlattices have been replaced by an effective $Al_{0.75}Ga_{0.25}N$:Mg hole injection layer and an $Al_{0.28}Ga_{0.72}N$:Mg hole transport layer. The p-side contact is on a GaN:Mg contact layer. The p-side Mg concentration is $N_A = 10^{19}$ cm^{-3} resulting in a free hole density $p \approx 2 \cdot 10^{16}$ cm^{-3} in the hole injection layer. The n-side Si concentration is $N_D = 4 \cdot 10^{18}$ cm^{-3}. The p side barrier and the quantum wells are unintentionally doped with a donor density $N_{\mathrm{D,uid}} = 5 \cdot 10^{16}$ cm^{-3} in accordance with experimental findings. The other barriers have a donor doping with a Si concentration of $N_D = 3 \cdot 10^{18}$ cm^{-3}. The Al mole faction in the QWs has been calibrated to match the experimental emission spectra. Two out of the three quantum wells have nominal emission at 233 nm wavelength while one quantum well emits at 250 nm wavelength. The permutations of the 250 nm QW position are denoted P for the p-side 250 nm QW, M for the middle 250 nm QW and N for the n-side 250 nm QW. With reference to the band structure in Fig. 1 the QW emitting near 250 nm is denoted as deep QW whereas the other QWs are denoted as shallow.

The carrier transport and luminescence in this structure are solved with a multi scale simulation approach. The entities of the solver and their interaction is schematically illustrated in Fig. 2. The momentum space models for quantization and the real space models for carrier transport are coupled by energy space models for carrier distribution, QW capture and IHB.

The QW carrier distribution is subject to the 6x6 wurtzite $\mathbf{k} \cdot \mathbf{p}$-Schrödinger model [15], [16] considering the electrostatic potential of the global Poisson equation. Luminescence is calculated with free carrier theory in the weak coupling approximation using the momentum matrix elements obtained from the $\mathbf{k} \cdot \mathbf{p}$ wave functions. Homogeneous broadening is included. This approach eliminates the need for calibrating a radiative recombination parameter B, inherently includes phase space filling as well as the quantum confined Stark effect, and discriminates TE and TM polarized emission which is crucial for comparison with characterization results.

The statistical alloy fluctuation seen through IHB is considered by a Gaussian broadening of the sub band energy levels [11] that enter the luminescence and phase space filling calculation. Though lateral non-equilibrium and quantization are neglected in contrast to the localized landscape model [17] the approach reproduces emission spectra including the degree of polarization well and facilitates self consistent and efficient IHB modelling. The IHB model affects the carrier distribution in energy space and thus the Fermi levels as well as the QW carrier capture [18].

To support non-equilibrium distributions in the vicinity of deep QWs [19] carriers are separated into as many bound populations as there are QWs and one global continuum population. Each of the populations is subject to a dedicated continuity equation. The QW populations are coupled to the continuum population by capture [18]. The self consistent radiative recombination due to the microscopic model enters the QW continuity equation in addition to non-radiative Shockley-Read-Hall (SRH) and Auger recombination. The SRH recombination is subject to the Shockley model [20] using the electron and hole SRH lifetimes as model parameters. The Auger electron (C_n) and hole (C_p) coefficient are model parameters for the Auger recombination calculation. The Auger recombination model is subject to the QW envelope wave function overlap [21], [22].

The envelope wave function calculated from the $\mathbf{k} \cdot \mathbf{p}$-Schrödinger solution gives rise to the QW carrier distribution in the transversal direction. The resulting charge distribution enters the global Poisson equation in addition to the continuum electron and hole charge. The piezoelectric and spontaneous polarization are reduced to 50% of the theoretical values [23] for the Poisson equation which is necessary to reproduce the experimental Stark

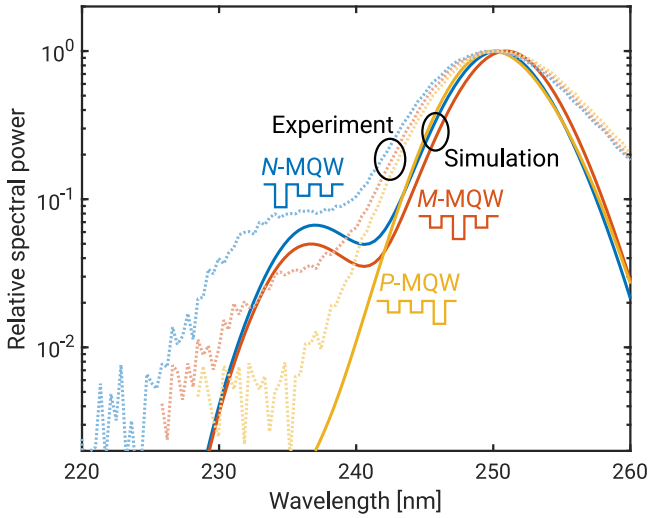

Fig. 3. Spectral calibration of the IHB and the shallow QW (233 nm) to deep QW (250 nm) luminescence distribution at $j = 13\ \mathrm{Acm}^{-2}$. The samples are denoted as N-MQW, M-MQW, and P-MQW for the n-side, middle, and p-side deep QW location, respectively. The shallow QW emission vanishes in the P-MQW. The spectral distribution can be reproduced for a barrier hole mobility $\mu_{\mathrm{h,bar}} \leq 0.2\,\mathrm{cm}^2/(\mathrm{Vs})$.

shift of the mean photon energy [24]. Doping is subject to incomplete ionization. The donor and acceptor ionization energies [7], [25] are subject to proximity reduction [5].

For a better modelling of barrier tunnelling and potential trap quantization of the continuum carriers a quantum correction is applied to the electrostatic potential [26]. The quantum corrected drift only affects the continuum carrier transport [13] but not the $\mathbf{k}\cdot\mathbf{p}$-Schrödinger wave functions. A Newton solver gives rise to the coupled solution of real and energy space models. Self consistency with the $\mathbf{k}\cdot\mathbf{p}$-Schrödinger model is achieved in a Gummel iteration.

III. Simulation Model Calibration

The simulation has been calibrated at room temperature matching the normalized experimental emission spectra by altering the QW composition and the IHB energy. Simulated emission spectra have been weighted with the light extraction efficiency (LEE) calculated for TE and TM-polarized emission by ray tracing [3]. Fig. 3 shows a comparison of the experimental and simulation results at $T = 300\,K$ and $j = 13\,\mathrm{Acm}^{-2}$ corresponding to $I = 20\,\mathrm{mA}$ in the experiment. In absence of a distinct short wavelength (233 nm) emission peak the N-, M-, and P-MQW allow only the spectral calibration of the deep QW. Therefore, the shallow QW emission has been calibrated for an LED with three short wavelength QWs. The broadening energies have been determined to $\sigma_d = 81$ meV for the deep QW and $\sigma_d = 110\,\mathrm{meV}$ for the shallow QWs. The broadening energy distributes not equally amongst the bands with the conduction band taking the major part due to the larger band offset [11]. When including the IHB the calibrated QW composition matches the experimental value well. Effects responsible for the Urbach tail [27] are not included in the broadening model resulting in a steeper low energy slope in the simulation.

The luminescence distribution seen through the characteristic emission spectra give rise to the transport analysis in the active region. The ratio of the shallow (233 nm) QW radiative recombination rate R_{s} to the deep (250 nm) QW radiative recombination rate R_{d} changes with the deep QW arrangement and enters also the model calibration. The P-MQW emission shows vanishing shallow QW emission in both experiment and simulation. The P-MQW does not facilitate transport analysis but serves as a benchmark for the simulation model and for spectral calibration.

Electron transport in AlGaN is subject to a doping and temperature dependent Arora mobility model [28]. In the intrinsic AlN EBL the hole mobility is $\mu_{\mathrm{h,EBL}} = 1\,\mathrm{cm}^2/(\mathrm{Vs})$ [6]. The hole mobility in the doped barriers is fitted to match the ratio $R_{\mathrm{s}}/R_{\mathrm{d}}$ for the N-MQW and M-MQW. The other fit parameter, the electron capture time of the deep QW, affects $R_{\mathrm{s}}/R_{\mathrm{d}}$ equally for the N-MQW and M-MQW. At room temperature, the N-MQW shows the highest short wavelength emission of all samples. This characteristic is reproduced in the simulation with a barrier hole mobility $\mu_{\mathrm{h,bar}} \leq 0.2\,\mathrm{cm}^2/(\mathrm{Vs})$. The role of the hole mobility for the transport is analyzed in Section IV.

Threading dislocation assisted SRH recombination [29] as well as Auger recombination are included as non-radiative recombination terms. The SRH electron and hole life times have been determined for a threading dislocation density $N_{\mathrm{td}} = 10^9\ \mathrm{cm}^{-2}$. In absence of calibrated Auger model parameters for AlGaN the parameters for InGaN/GaN quantum wells have been used [22]. This is in accordance with the finding that the ABC model Auger coefficients are similar for AlGaN and InGaN [30]. The contribution of non-radiative recombination might differ in deep and shallow QWs but has no large effect on the difference between the N-MQW and the M-MQW shallow QW emission. Apart from the LEE the transport related CIE is the dominant loss mechanism in the high current regime [3].

IV. DUV MQW Active Region Transport

With the calibrated model we investigate the transport in the active region of the mixed MQW LED and discuss the impact of the model parameters. Fundamental transport properties can be deduced from the band diagram in Fig. 1 comparing the N-MQW and P-MQW. As noted in Section III the short wavelength emission vanishes in the P-MQW. Simulations show that R_{s} is at least by three order of magnitude lower than R_{d} independent of the chosen model parameters. The hole quasi Fermi level gradient in p-side barrier suggests that hole injection is subject to a barrier of $\Delta E_{\mathrm{Fp}} \approx 250\,\mathrm{meV}$ in the N-MQW. The polarization field at the n-side deep QW creates another barrier. In the P-MQW the p-side hole barrier is even higher and the p-side deep QW acts as hole trap. The polarization field induced VB barrier between the p-side and mid QW impedes the hole accumulation the mid and n-side shallow QW. The recombination in the QWs is not limited by hole capture because the continuum and bound (QW) hole quasi Fermi levels match meaning that holes are in thermal equilibrium.

Electron injection into and electron distribution in the active region is not obstructed by a barrier. The continuum electron quasi Fermi level in Fig. 1 is nearly flat from the n-side to the

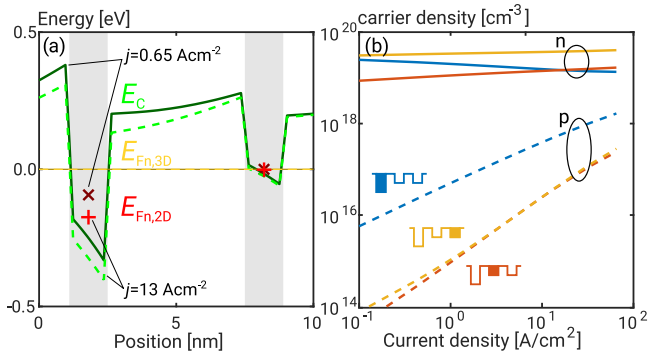

Fig. 4. Left: Conduction band (CB) near the n-side and mid QW of the N-MQW at $j = 0.65\,\mathrm{Acm}^{-2}$ (solid) and $j = 13\,\mathrm{Acm}^{-2}$ (dashed). The thin lines illustrate the continuum electron quasi Fermi level. The markers are the bound electron quasi Fermi levels at $j = 0.65\,\mathrm{Acm}^{-2}$ ($\times$) and $j = 13\,\mathrm{Acm}^{-2}$ ($+$). The continuum electron quasi Fermi level does not shift with the current because it is tied to the n-contact reference potential. Instead the CB edge shifts. Right: Electron (solid) and hole (dashed) density in each QW versus the current j.

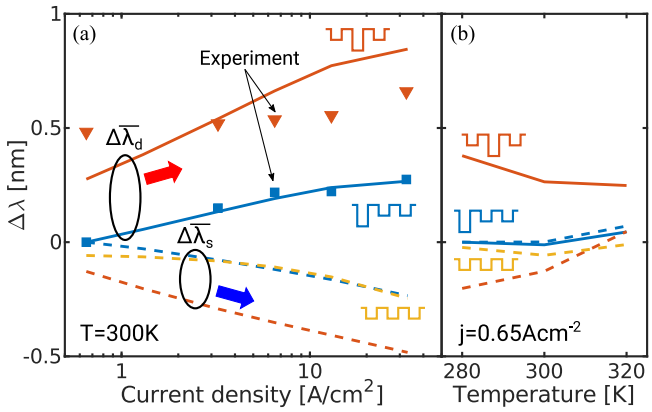

Fig. 5. Left: Shift of the emission wavelength expectation value $\Delta\overline{\lambda_d}$ and $\Delta\overline{\lambda_s}$ with the current density j at $T = 300$K for the N- and M-MQW. The solid markers illustrate the experimental results. Right: Shift of the emission wavelength expectation value $\Delta\overline{\lambda_d}$ and $\Delta\overline{\lambda_s}$ with the temperature at $j = 0.65\,\mathrm{Acm}^{-2}$.

active region showing only a gradient in the EBL. The barrier donor doping mitigates the polarization fields by screening and enables a constantly high electron density in the QWs as illustrated in Fig. 4(b) enhancing the electron injection. Due to the high electron density the relative contribution of non-radiative recombination does not change as much with the current as in an intrinsic active region [31]. An increase of the recombination rate with the current is seen through an increase of the QW hole density.

The CB detail of the N-MQW in Fig. 4(a) shows that electrons in the shallow QWs are in thermal equilibrium. The recombination there is not limited by capture, but the QW electron density is limited by the continuum density showing only a minor increase with the current as depicted in Fig. 4(b). The p-side QW accommodates a slightly higher electron density than the mid QW because of the lower sub band levels. Fig. 1 illustrates that the CB near the mid and p-side QW differs because of the intrinsic p-side barrier.

In the deep QW electrons are not in thermal equilibrium. The quasi Fermi level difference between continuum and bound states increases from $E_{\mathrm{Fn,3D}} - E_{\mathrm{Fn,2D}} \approx 4k_BT$ at $j = 0.65\,\mathrm{Acm}^{-2}$ to $E_{\mathrm{Fn,3D}} - E_{\mathrm{Fn,2D}} \approx 8k_BT$ at $j = 13\,\mathrm{Acm}^{-2}$. Thus, recombination in the deep QW is limited by electron capture seen through a decrease of the electron density while the hole density increases with the current. The cumulative change in the space charge causes a negative shift of the CB and VB near the deep QW impeding the hole injection into the deep QW. This explains the lower hole density gradient for the deep QW compared to the shallow QWs in Fig. 4(b). It is noted that the charge in the deep QW does not screen the polarization field because its small width and high depth reduce the wave function and thus charge asymmetry. Bands do not shift near the shallow QWs because there is only a minor change of the space charge with the current. The QW electron density is nearly pinned there and the hole density is not high enough to significantly change the electrostatic potential.

The deep QW emission shows a small red shift $\Delta\overline{\lambda_d}$ with increasing current both in experiment and simulation which already exists in the low current regime. The expectation value of the emission wavelength in the N- and M-MQW is illustrated in Fig. 5(a). The spectral shift of the shallow QWs cannot be determined experimentally at room temperature but the simulation shows a small blue shift $\Delta\overline{\lambda_s}$ with increasing current as it would be expected considering the CB phase space filling [32]. Both shifts are minor, though, because the electron density in the active region is pinned in the presence of the barrier donor doping. The red shift by self heating expected to $\Delta T \leq 20$ K does not provide a sufficient explanation. Simulations in Fig. 5(b) show only a minor emission wavelength shift with temperature which cannot account for the observed shift. The reduction of the bound electron density in the deep QW with rising current provides a sufficient explanation for the red shift. The decreasing electron density is seen though a decrease of the mean electron energy which occurs as a small red shift in the spectrum. Thus, the observed red shift presents an indirect evidence for the non-equilibrium electron distribution near the deep QW.

The barrier hole mobility has been determined to $\mu_{\mathrm{h,bar}} \leq 0.2\,\mathrm{cm}^2/(\mathrm{Vs})$ to match the experimental results. This value is not out of range considering that the hole mobility in Mg doped AlGaN takes values as low as $\mu_h \approx 10^{-3}\,\mathrm{cm}^2/(\mathrm{Vs})$ [6]. The effect of the hole mobility in the barriers and the EBL is presented in Fig. 6. The barrier hole mobility affects particularly the hole distribution in the active region but is not critical for the CIE.

It appears inconsistent that the deep QW in n-side position accounts for more than 80% of the total emission despite the low hole mobility. Fig. 6(a) illustrates that this fraction indeed decreases with the hole mobility. According to Fig. 4(b) the hole density in the deep QW is by at least one order of magnitude higher than in the shallow QWs for $\mu_{\mathrm{h,bar}} \leq 0.2\,\mathrm{cm}^2/(\mathrm{Vs})$, though. This hole accumulation at a comparable electron density explains the dominant radiative recombination from the deep QW. The much higher hole density results from the deep QW acting as a VB trap even in the n-side position due to the larger band offsets and the polarization potential. The deep QW hole

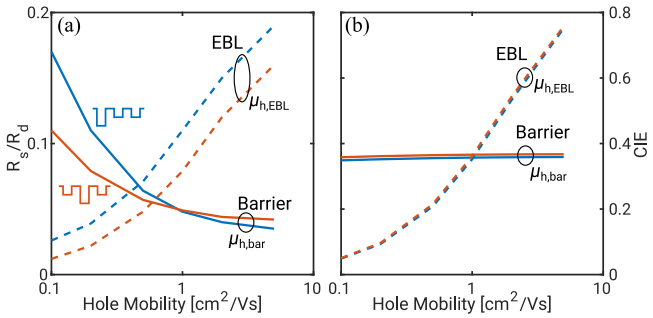

Fig. 6. Left: Effect of the barrier and EBL hole mobility $\mu_{\mathrm{h,bar}}$ and $\mu_{\mathrm{h,EBL}}$ on the luminescence distribution ratio $R_{\mathrm{s}}/R_{\mathrm{d}}$ for the N- and M-MQW. Right: Effect of the hole mobility on the CIE.

drain limits hole accumulation in the shallow QWs and therefore the shallow QW emission. As previously discussed, the deep QW acts in any case as a hole barrier so that the emission of any shallow QW closer to the n-side vanishes.

The low hole mobility in the barriers does not severely impede the hole distribution in the active region. Holes are evenly distributed amongst the shallow QWs of the N-MQW as shown in Fig. 4(b). The quasi Fermi level $E_{\mathrm{Fp,3D}}$ in Fig. 1 shows a small hole barrier in the N-MQW between the mid and n-side QW, but this barrier is not high enough to limit the recombination current though the deep QW. The hole barrier seen though the quasi Fermi level gradient in the EBL and the p-side barrier is much higher. In conclusion, the small hole mobility is not very critical for the re-distribution of holes in the active region but a small hole mobility is very critical for the hole injection into the active region and thus the CIE.

In absence of alloy, ionized impurity, and neutral impurity scattering the hole mobility in pure AlN and thus the EBL is higher than the barrier hole mobility. Fig. 6 demonstrates that particularly the EBL hole mobility is critical for the hole injection and thus the CIE. It changes the luminescence re-distribution of the N- and M-MQW in the same way, though, and therefore does not contribute to the effect of the barrier mobility. While the barrier hole mobility has virtually no effect on the CIE it might have an indirect effect on the internal quantum efficiency by controlling the luminescence re-distribution amongst the quantum wells of an MQW. An equal luminescence distribution mitigates the droop in presence of Auger recombination.

V. Conclusion

The optimization of the quantum yield of deep ultraviolet light emitting diodes is hampered by the opaque active region physics in these devices. In this context we have demonstrated the analysis of the emission spectra of a deep ultraviolet mixed multi quantum well light emitting diode by physics based simulation to unravel the otherwise opaque carrier transport in the active region. The physics based simulation model couples a $\mathbf{k}\cdot\mathbf{p}$-Schrödinger solver for the luminescence and carrier distribution in the quantum wells with a semi-classical drift diffusion transport solver and has been refined to meet the luminescence and transport physics in III-Nitride multi quantum well light emitting diodes.

With the luminescence and transport solver we have analyzed the characteristic emission spectra of the mixed quantum well light emitting diodes serving as markers for the carrier transport in the active region. From the emission spectra we deduce figures of the hole mobility in the barriers of the active region. Though the hole mobility in the donor doped barriers is low it does not significantly impede the re-distribution of holes in the active region. A low hole mobility in the electron blocking layer is more critical because it limits the hole injection. We have have found evidence for a non-equilibrium distribution of electrons near the deep quantum well of the mixed multi quantum well light emitting diodes. Electrons in the shallow quantum wells and holes have been found to be in thermal equilibrium with the continuum electrons and holes, respectively. We have further demonstrated the relevance of the EBL hole mobility for the carrier injection efficiency. The findings can enter the physical model calibration for the hole injection efficiency optimization in deep ultraviolet light emitting diodes.

References

[1] M. Kneissl, T.-Y. Seong, J. Han, and H. Amano, "The emergence and prospects of deep-ultraviolet light-emitting diode technologies," *Nature Photon.*, vol. 13, no. 4, pp. 233–244, 2019. [Online]. Available: https://www.nature.com/articles/s41566-019-0359-9

[2] H. Amano et al., "The 2020 UV emitter roadmap," *J. Phys. D: Appl. Phys.*, vol. 53, no. 50, 2020, Art. no. 503001, doi: 10.1088/1361-6463/aba64c.

[3] M. Guttmann et al., "Optical light polarization and light extraction efficiency of AlGaN-based LEDs emitting between 264 and 220 nm," *Japanese J. Appl. Phys.*, vol. 58, Jun. 2019, Art. no. SCCB20, doi: 10.7567/1347-4065/ab0d09.

[4] K. B. Nam, M. L. Nakarmi, J. Li, J. Y. Lin, and H. X. Jiang, "Mg acceptor level in AlN probed by deep ultraviolet photoluminescence," *Appl. Phys. Lett.*, vol. 83, pp. 878–880, 2003. [Online]. Available: https://scitation.aip.org/content/aip/journal/apl/83/5/10.1063/1.1594833

[5] S. Brochen, J. Brault, S. Chenot, A. Dussaigne, M. Leroux, and B. Damilano, "Dependence of the Mg-related acceptor ionization energy with the acceptor concentration in p-type GaN layers grown by molecular beam epitaxy," *Appl. Phys. Lett.*, vol. 103, no. 3, 2013, Art. no. 032102. [Online]. Available: https://link.aip.org/link/APPLAB/v103/i3/p032102/s1&Agg=doi

[6] N. H. Tran, B. H. Le, S. Zhao, and Z. Mi, "On the mechanism of highly efficient p-type conduction of Mg-doped ultra-wide-bandgap AlN nanostructures," *Appl. Phys. Lett.*, vol. 110, no. 3, Jan. 2017, Art. no. 032102, doi: 10.1063/1.4973999.

[7] F. Mehnke et al., "Electronic properties of Si-doped Al $_x$ Ga$_{1-x}$N with aluminum mole fractions above 80%," *J. Appl. Phys.*, vol. 120, no. 14, Oct. 2016, Art. no. 145702. [Online]. Available: https://pubs.aip.org/aip/jap/article/567915

[8] L. Rigutti et al., "Statistical nanoscale study of localised radiative transitions in GaN/AlGaN quantum wells and AlGaN epitaxial layers," *Semicond. Sci. Technol.*, vol. 31, no. 9, Sep. 2016, Art. no. 095009. [Online]. Available: https://stacks.iop.org/SST/31/095009/mmedia

[9] C. Frankerl et al., "Carrier dynamics in Al-rich AlGaN/AlN quantum well structures governed by carrier localization," *Phys. Status Solidi (B)*, vol. 257, no. 12, Dec. 2020, Art. no. 2000242, doi: 10.1002/pssb.202000242.

[10] C. Mounir et al., "Impact of inhomogeneous broadening on optical polarization of high-inclination semipolar and nonpolar In $_x$ Ga$_{1-x}$N/GaN quantum wells," *Phys. Rev. B*, vol. 93, no. 23, Jun. 2016, Art. no. 235314, doi: 10.1103/PhysRevB.93.235314.

[11] F. Römer, M. Guttmann, T. Wernicke, M. Kneissl, and B. Witzigmann, "Effect of inhomogeneous broadening in ultraviolet III-Nitride light-emitting diodes," *Materials*, vol. 14, no. 24, 2021, Art. no. 7890, doi: 10.3390/ma14247890.

[12] B. Galler et al., "Investigation of the carrier distribution in InGaN-based multi-quantum-well structures," *Phys. Status Solidi (C)*, vol. 8, no. 7/8, pp. 2372–2374, Jul. 2011, doi: 10.1002/pssc.201001075.
[13] F. Römer and B. Witzigmann, "Luminescence distribution in the multi-quantum well region of III-nitride light emitting diodes," *Proc. SPIE*, vol. 10124, 2017, Art. no. 101240Y, doi: 10.1117/12.2253668.
[14] J. Höpfner et al., "Unravelling carrier transport in far-UVC LEDs by temperature dependent electroluminescence measurements," unpublished.
[15] S. Chuang and C. Chang, "Kp method for strained Wurtzite semiconductors," *Phys. Rev. B*, vol. 54, no. 4, Jul. 1996, Art. no. 2491, doi: 10.1103/PhysRevB.54.2491.
[16] S.-H. Park and S.-L. Chuang, "Crystal-orientation effects on the piezoelectric field and electronic properties of strained wurtzite semiconductors," *Phys. Rev. B*, vol. 59, no. 7, pp. 4725–4737, Feb. 1999, doi: 10.1103/PhysRevB.59.4725.
[17] C. K. Li et al., "Localization landscape theory of disorder in semiconductors. III. Application to carrier transport and recombination in light emitting diodes," *Phys. Rev. B*, vol. 95, no. 14, 2017, Art. no. 144206, doi: 10.1103/PhysRevB.95.144206.
[18] G. Baraff, "Semiclassical description of electron transport in semiconductor quantum-well devices," *Phys. Rev. B*, vol. 55, no. 16, 1997, Art. no. 10745. [Online]. Available: https://prb.aps.org/abstract/PRB/v55/i16/p10745_1
[19] A. Shedbalkar and B. Witzigmann, "Non equilibrium Green's function quantum transport for green multi-quantum well nitride light emitting diodes," *Opt. Quantum Electron.*, vol. 50, no. 2, pp. 1–10, 2018, doi: 10.1007/s11082-018-1335-1.
[20] W. Shockley and W. Read Jr., "Statistics of the recombinations of holes and electrons," *Phys. Rev.*, vol. 87, no. 5, pp. 835–842, 1952. [Online]. Available: https://prola.aps.org/abstract/PR/v87/i5/p835_1
[21] E. Kioupakis, Q. Yan, and C. G. V. d. Walle, "Interplay of polarization fields and Auger recombination in the efficiency droop of nitride light-emitting diodes," *Appl. Phys. Lett.*, vol. 101, no. 23, 2012, Art. no. 231107, doi: 10.1063/1.4769374.
[22] F. Römer and B. Witzigmann, "Effect of Auger recombination and leakage on the droop in InGaN/GaN quantum well LEDs," *Opt. Exp.*, vol. 22, no. S6, 2014, Art. no. A1440. [Online]. Available: https://www.opticsinfobase.org/abstract.cfm?URI=oe-22-S6-A1440
[23] O. Ambacher et al., "Pyroelectric properties of Al(In)GaN/GaN hetero- and quantum well structures," *J. Phys.: Condens. Matter*, vol. 14, no. 13, pp. 3399–3434, Apr. 2002. [Online]. Available: https://iopscience.iop.org/0953-8984/14/13/302
[24] M. Sabathil, A. Laubsch, and N. Linder, "Self-consistent modeling of resonant PL in InGaN SQW LED-structure," in *Light-Emitting Diodes: Research, Manufacturing, and Applications XI*, vol. 6486. Bellingham, WA, USA: SPIE, 2007, pp. 212–220, doi: 10.1117/12.700461.
[25] Y. Taniyasu, M. Kasu, and T. Makimoto, "An aluminium nitride light-emitting diode with a wavelength of 210 nanometres," *Nature*, vol. 441, no. 7091, pp. 325–328, May 2006. [Online]. Available: https://www.ncbi.nlm.nih.gov/pubmed/16710416
[26] D. Ferry, S. Ramey, L. Shifren, and R. Akis, "The effective potential in device modeling: The good, the bad and the ugly," *J. Comput. Electron.*, vol. 1, pp. 59–65, 2002. [Online]. Available: https://link.springer.com/article/10.1023/A:1020763710906
[27] M. Piccardo et al., "Localization landscape theory of disorder in semiconductors. II. Urbach tails of disordered quantum well layers," *Phys. Rev. B*, vol. 95, no. 14, pp. 1–12, 2017, doi: 10.1103/PhysRevB.95.144205.
[28] M. Farahmand et al., "Monte Carlo simulation of electron transport in the III-nitride Wurtzite phase materials system: Binaries and ternaries," *IEEE Trans. Electron Devices*, vol. 48, no. 3, pp. 535–542, Mar. 2001. [Online]. Available: https://ieeexplore.ieee.org/xpls/abs_all.jsp?arnumber=906448
[29] S. Y. Karpov and Y. N. Makarov, "Dislocation effect on light emission efficiency in gallium nitride," *Appl. Phys. Lett.*, vol. 81, no. 25, pp. 4721–4723, 2003, doi: 10.1063/1.1527225.
[30] F. Nippert et al., "Auger recombination in AlGaN quantum wells for UV light-emitting diodes," *Appl. Phys. Lett.*, vol. 113, no. 7, Aug. 2018, Art. no. 071107, doi: 10.1063/1.5044383.
[31] H. Masui, "Diode ideality factor in modern light-emitting diodes," *Semicond. Sci. Technol.*, vol. 26, no. 7, Jul. 2011, Art. no. 075011. [Online]. Available: https://stacks.iop.org/0268-1242/26/i=7/a=075011
[32] B. Witzigmann, F. Römer, T. Wernicke, M. Guttmann, M. Kneissl, and N. Susilo, "Inhomogeneous spectral broadening in deep ultraviolet light emitting diodes," in *Physics and Simulation of Optoelectronic Devices XXVII*, M. Osiński, Y. Arakawa, and B. Witzigmann, Eds., vol. 10912. Bellingham, WA, USA: SPIE, 2019, pp. 18–26, doi: 10.1117/12.2512182.